Fifteen Years of (Major to Great) Tsunamigenic Earthquakes

F Romano, S Lorito, and A Piatanesi, Istituto Nazionale di Geofisica e Vulcanologia, Roma, Italy
T Lay, Earth and Planetary Sciences Department, University of California Santa Cruz, Santa Cruz, CA, United States

Tsunamis, Seismically Induced

Tsunamis are a series of long gravity waves generated by the displacement of a significant volume of water that propagating in the sea, under the action of the gravity force, returns in its original equilibrium position. Differently from the common wind waves, tsunamis are characterized by large wavelengths (ranging from tens to hundreds of km) and long periods (ranging from minutes to hours).

Several natural phenomena such as earthquakes, landslides, volcanic eruptions, the rapid change of atmospheric pressure (meteotsunami), or asteroids impacts can be the source of a tsunami; among these, the most frequent is represented by the earthquakes.

Most of the very tsunamigenic earthquakes occur nearby the Earth convergent boundaries (Fig. 1), at the subduction zones, where the oceanic plate underthrust the continental one. During the last 15 years (2004–19), subduction zones hosted a particularly high number of tsunamigenic earthquakes, though consistent with the normal seismicity rate statistical fluctuations (Lay, 2015), with catastrophic consequences in terms of casualties and damages. The impact of a tsunami can be indeed particularly severe in terms of fatalities, people missing, building destruction, and damages to infrastructures (e.g., ports, power plants, dams). The largest tsunamis since 2004 were those ensuing from the 2004 M_w 9.2 Sumatra-Andaman (Indonesia) and the 2011 M_w 9.0 Tohoku (Japan) earthquakes (e.g., Lorito et al., 2016), causing 220,000+ and 15,000+ victims, respectively.

Subduction tsunamigenic earthquakes can be classified in three big classes (Fig. 2): "ordinary" intraplate (i.e., occurring at the plate interface), intraplate (i.e., occurring within the subducting slab, within the overlying crust or at the outer rise), and "tsunami earthquakes" (i.e., interplate events generating a tsunami larger than expected for their magnitude).

When an earthquake occurs, the dislocation along the fault plane generates a deformation of the surrounding medium (the Earth's crust); if the earthquake occurs in the open sea or close enough to the coast, then the seafloor may be deformed. It is principally the vertical seafloor deformation that perturbs the equilibrium of the whole water column above and triggers the tsunami. The sea waves generated in this way propagate over the sea at long distances almost without any dissipation, since they are long waves due to the typical hundreds of kilometers scale wavelength related to the earthquake fault size (mainly the fault width).

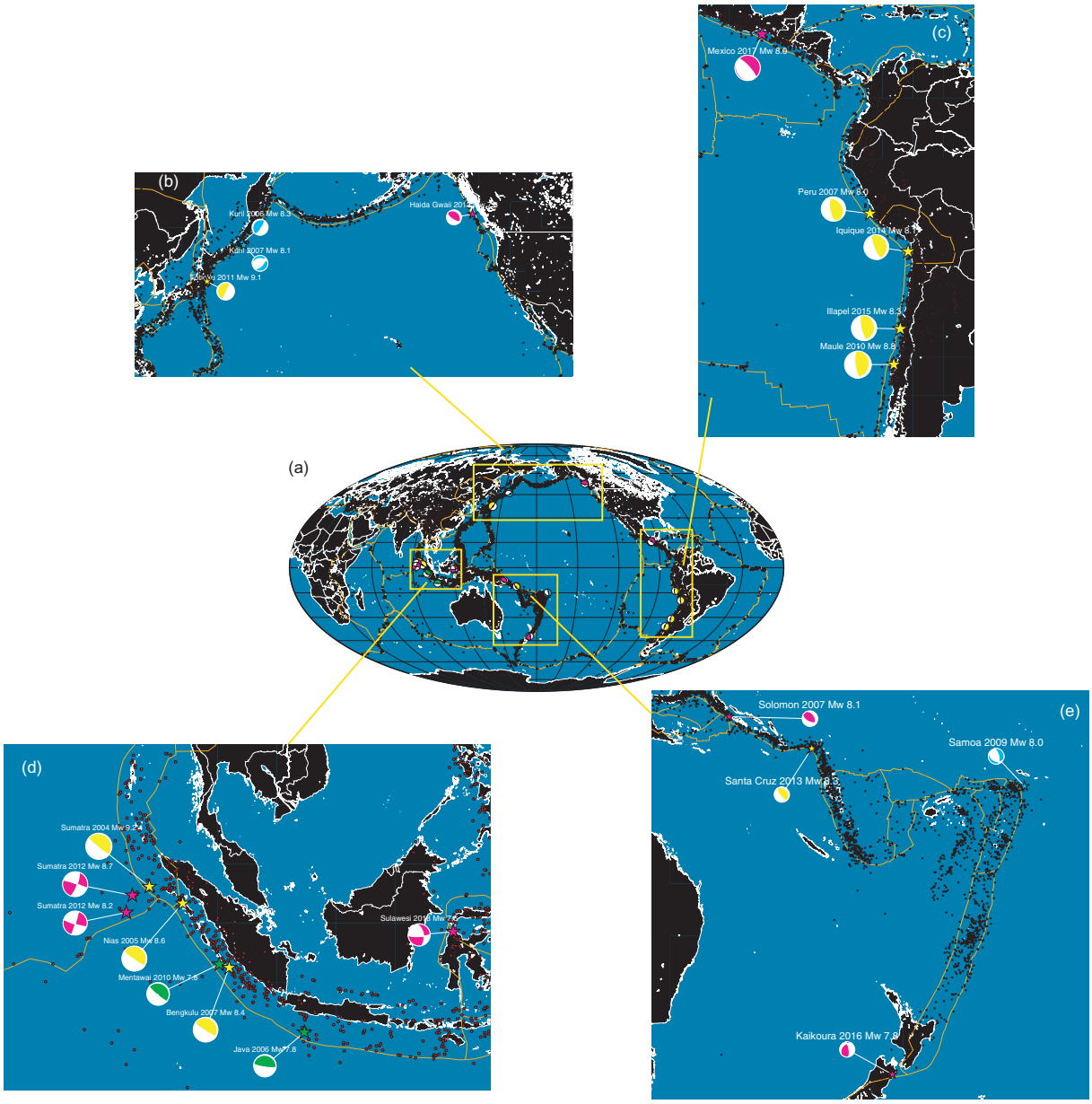

Fig. 1 Panel (a) Location map of the global seismicity showing earthquakes with magnitude greater than 6.0 (USGS catalogue). Panels (b–e) are close-up views where are plotted the locations and the focal mechanism (i.e., represented by the beach ball) of the major to great earthquakes occurred in the period 2004–19; in particular, the different colors of stars (i.e., the epicenter) and beach balls indicate megathrust (yellow), doublets (cyan), tsunami earthquakes (green), and special events (magenta).

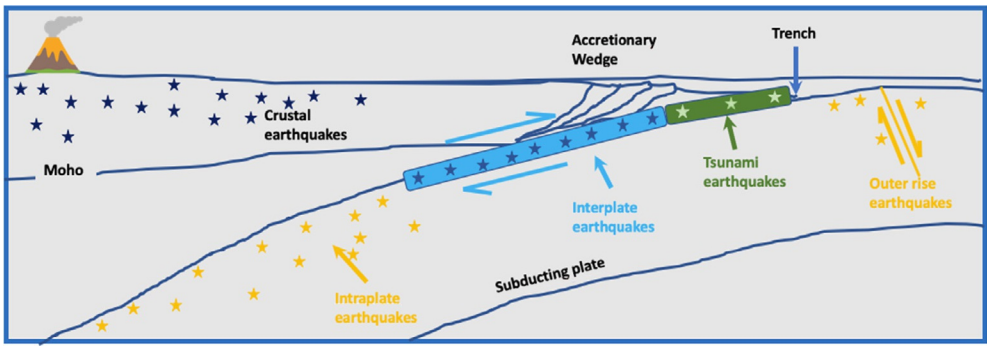

Fig. 2 Sketch showing the different classes of subduction earthquakes.

The size of the tsunami is, on the first order, related to the seismic moment (or equivalently the magnitude) of the earthquake; the larger the magnitude the bigger the associate tsunami. For a given fault and faulting mechanism, the coseismic deformation, is approximately linearly dependent on the fault dislocation (or slip, that is the relative movement between the downgoing – footwall - and the overlying – hanging wall – plates). Thus, the bigger the magnitude, the larger the slip, and the more pronounced the vertical seafloor deformation, resulting in a bigger tsunami. However, the distribution of vertical seafloor coseismic displacement, particularly in the near field of the tsunami source, depends not only on the earthquake magnitude but also on the focal depth, faulting mechanism, and the heterogeneity of the slip distribution, which all together determine basic wave features as amplitude and period/wavelength.

In the near field, the relationship between slip distribution and tsunami characteristics (such as the runup, that is the highest topographic elevation reached by the tsunami during the inundation stage) is even more complicated and may also depend on the position and orientation of the source with respect to the coast, the amount of water above the tsunamigenic source, and by the coupling of the morphological features of the coast with the tsunami.

Fifteen Years of Major to Great Tsunamigenic Earthquakes

The last 15 years were characterized by a large number of great earthquakes ($M_w > 8$) (Lay, 2015), most of which occurred in subduction zones. Significant tsunamis were generated by most of these great events as well as by several major (M_w 7.0–7.9) earthquakes hosted along the shallow part of subduction megathrust, or by great intraplate normal faulting events near subduction zones.

Among these, the 2004 Sumatra-Andaman M_w 9.2 and the 2011 Tohoku M_w 9.0 earthquakes are, respectively, the third and the fourth largest earthquakes seismologically recorded (since 1900); previously, the largest megathrust earthquakes seismologically recorded were the 1952 M_w 9.0 Kamchatka, the 1964 M_w 9.2 Alaska, and the 1960 M_w 9.5 Chile events (Kanamori, 1977). All of these earthquakes generated transoceanic tsunamis in the Pacific and Indian ocean.

Some of these megathrust events featured ruptures with surprising spatial extent and characteristics of their slip distribution, controlling the feature of the tsunamis they generated. In particular, the magnitudes of the Sumatra-Andaman and the Tohoku earthquakes, which produced two of the most damaging tsunamis in modern times, were larger than had been anticipated for their source regions. Now it is widely accepted that great tsunamigenic earthquakes may occur in most subduction zones worldwide, although very infrequently in some regions (e.g., Stein and Okal, 2011; Kagan and Jackson, 2013).

The Indian Ocean earthquake and tsunami caught us unprepared because of the lack of knowledge of its predecessors (subsequently discovered, Sieh et al., 2015) and to the widely accepted assumptions regarding the relatively low seismic potential of old oceanic plates featuring highly oblique convergence. This earthquake generated a huge tsunami that propagated over the Indian Ocean and even into the Pacific and Atlantic Oceans (Titov et al., 2005). The overall rupture length (>1300 km on the Sunda Trench from Northern Sumatra to the Andaman Islands) and duration (>8 min) of the 2004 M_w 9.2 Sumatra-Andaman megathrust earthquake were moreover totally unexpected.

Also the 2011 M_w 9.0 Tohoku earthquake was larger than anticipated at its location; also in this case, perhaps, only incomplete information regarding prior earthquakes was available, and partially in the incorrect assumptions concerning fault segmentation and the likely maximum magnitude derived from convergence rate and crustal age (Stein and Okal, 2011). A huge and devastating transoceanic tsunami was generated, enhanced by the very large and shallow amount of slip in the trench zone (>50 m), probably never clearly observed before. So much coseismic slip at shallow depths was very surprising. The shallow part of the megathrust is characterized by the presence of the sedimentary accretionary wedge. Hence, the region nearby the trench axis is or was commonly thought not capable of accumulating significant elastic strain. Rather, it can be described in terms of frictional behavior as a velocity strengthening zone, thus favoring aseismic creep rather than stick-slip earthquake failure (e.g., Wang and Kinoshita, 2013).

Other major to great earthquakes occurred in the same time frame were crucial to better understand the complexity of the coseismic rupture and tsunamigenesis. For example, a better observational data basis was gained regarding the 'tsunami earthquakes,' which are very shallow events generally featuring $M_w < 8$, highlighted that they can generate (at least) regional tsunamis larger than expected for their moment magnitude. Earthquake doublets demonstrated triggering interactions between two regional fault systems, while events located in complicated tectonic environments, such as deformed slabs or triple plate junctions, illustrated the difficulty of anticipating tsunami excitation (e.g., Lay, 2015; Lorito et al., 2016).

The Study of Tsunamigenic Earthquakes

The study of the earthquake rupture process is one of the most important topics in seismology because it allows to reconstruct the image and the history of the dislocation along the fault plane during a seismic event. This is very important because can help to better constrain both the seismic and tsunami hazard assessment and the risk mitigation, for example with tsunami warning systems. Of course, a primary purpose is to better understand the physics behind the process and the parameters that control the tsunamigenic potential.

The common way to investigate the rupture process of an earthquake is through the inversion of geophysical data; the main purpose is to retrieve the kinematic rupture process of the event (i.e., slip, rake, rise-time, rupture velocity). Hence, the continuous

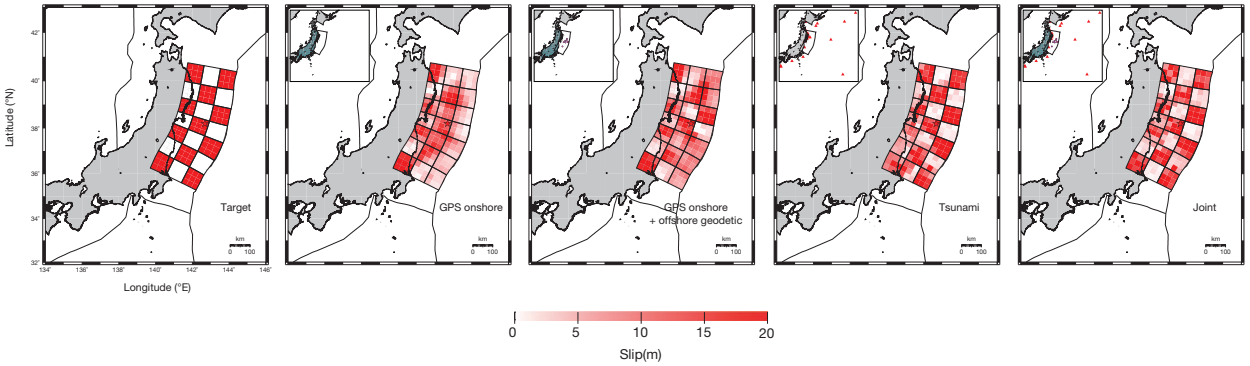

Fig. 3 Resolution test for the 2011 Tohoku earthquake (Romano et al., 2012). The panels, from left to right, show the target slip pattern to be recovered, the slip distributions estimated by inverting separately GPS data, jointly GPS and seafloor geodetic data, tsunami data; the figures show that the slip distribution estimated through geodetic data improves when are used both inland and offshore sensors if compared to the GPS only inversion, whereas the best result is obtained when geodetic and tsunami data are jointly inverted (last panel on the right).

increase and development of seismological, geodetic and tsunami networks allowed to investigate a number of tsunamigenic events occurred in the last 2 decades, and to illuminate the details of their seismic ruptures.

However, since the solution of problem is generally non-unique, a-priori constraints (e.g., fixed geometry parameterization) and regularization techniques are also used in the inversion scheme (e.g., Das, 2011). The inverse problem is commonly solved by using the linear least-squares method (e.g., Satake, 2009) or global optimization algorithms (e.g., the simulated annealing, Piatanesi and Lorito, 2007).

The data that can be used in the inversion depend mostly on the earthquake size and the available instruments that recorded it. Seismic waveforms from networks at global scale are commonly used to study the rupture process of all moderate to great earthquakes; otherwise, if the earthquake source occurs close to the instrumental network then strong-motion and geodetic data (e.g., GPS, InSAR, land leveling) may be available. If a tsunami is generated, tsunami waveforms recorded by tide gauges, bottom pressure sensors, and GPS buoys may be available for constraining the tsunami source.

Each kind of data, also depending on the earthquake and the mutual distance between seismic event and instrument, allows to image distinctly a specific feature of the rupture; for example, seismic waveforms are sensitive to the fault orientation and the rupture time history, whereas tsunami data are more sensitive to the spatial heterogeneities of the slip pattern; at the same time, for tsunamigenic subduction earthquakes, geodetic data well resolve the details of the coseismic rupture landward, while they are less sensitive offshore (Fig. 3). It appears clear then that the proper way to deal with the study of the seismic source, particularly for tsunamigenic earthquakes, is to exploit the complementary resolving powers of each kind of instrument/dataset in a joint inversion.

We will describe in the next paragraphs the most tsunamigenic earthquakes occurred in the period 2004–19. We divided them into different macro classes, that is: megathrust, doublets, tsunami earthquakes, and special tsunamigenic earthquakes.

Megathrust Tsunamigenic Earthquakes

The Sunda 2004–10 Sequence in the Indian Ocean

A sequence of tsunamigenic earthquakes occurred along the Sunda megathrust from 2004 to 2010. Three of these events were great megathrust earthquakes (M_w 9.2 2004 Sumatra-Andaman, M_w 8.6 2005 Nias, M_w 8.4 2007 Bengkulu), and will be descried in this section. Four had magnitude in the range M_w 7.6–7.9, two of which were classified as tsunami earthquakes; the latter are treated in a following section.

The Sumatra-Andaman megathrust earthquake, whose magnitude was M_w 9.2, has been one of the five greatest earthquakes recorded in the instrumental era. The epicenter (95.85°E, 3.32°N) was located ~80 km off the north-western coast of Sumatra island, and its rupture propagated northward for ~1300 km, causing a devastating tsunami in the Indian Ocean.

This event has been deeply studied by using different kind of data (teleseismic, tsunami, GPS, satellite altimetry), and its source model has been estimated through different inversion techniques to better investigate the slip and the long rupture duration (a comprehensive review can be found in Shearer and Bürgmann, 2010). Probably also because inversion techniques had not been tested before on such large events, there is not a full agreement among the estimated slip models, in terms of maximum fault dislocation (ranging from 11 to 35 m), rupture velocity (ranging from 1 to 4 km/s), and the occurrence of slip in the very shallow part of the megathrust, where some authors suggest the rupture of a splay fault to account for the huge runup (50 m, Choi et al., 2006) observed in Banda Aceh (Plafker et al., 2006); in this area the tsunami was devastating and penetrated more than 2 km inland. The impact of the tsunami was not confined only in Indonesia (average runup of 10 m), but was extensive in many countries: Thailand (average runup ~5 m), Sri Lanka (average runup ~5 m), India (average runup ~4 m), even in Somalia (runup ~10 m in some places), Bangladesh, Malaysia, Maldives, and Seychelles Islands. Furthermore, the tsunami generated by the 2004 Sumatra-Andaman earthquake was the first tsunami to be measured by tide gauges at global scale.

The March 28, 2005 Nias M_w 8.6 earthquake occurred just 3 months after the 2004 Sumatra-Andaman event; the epicenter (97.15°E, 2.09°N) was located between the Nias and Simeulue Islands, 200 km southeast from the great 2004 earthquake epicenter. Several studies, using teleseismic, GPS, and coral displacement data (e.g., Briggs et al., 2006; Hsu et al., 2011; Konca et al., 2007), are quite in agreement proposing a source model featuring two main patches of slip (maximum ~12 m) mainly located under Nias and southern Simeulue Islands. The location of the slip (deep and mainly located under the islands) mitigated the ensuing tsunami that was moderate despite the great earthquake magnitude (e.g., Geist et al., 2006). Indeed, the maximum measured runup, observed along the coast of Simeulue Island, was ~4 m.

The third megathrust earthquake of the period 2004–10 occurred on September 12, 2007, with the epicenter (101.37°E, 4.44°S) located ~130 km offshore from the city of Bengkulu. The source models of the M_w 8.4 Bengkulu earthquake (estimated through teleseismic, GPS, coral uplifts, InSAR, and tsunami data inversions, e.g., Lorito et al., 2008) share a rupture pattern propagating from the epicenter toward South Pagai Island (maximum slip ~7–12 m). As for the Nias earthquake, the depth of the slip played a role in the tsunamigenesis; actually, the ensuing tsunami was moderate with runup measured <4 m (Borrero et al., 2009).

Peru 2007

The subduction interface between the Nazca and South American Plates hosted on August 15, 2007, an M_w 8.0 earthquake. The hypocenter was located offshore of central Peru (76.60°W, 13.39°S) at a depth of ~40 km, ~60 km west from the city of Pisco.

The earthquake rupture process has been studied through teleseismic (Lay et al., 2010b) and InSAR (Sladen et al., 2010) data. The estimated slip distribution features two main patches of slip, one near the epicenter and the other located in the southwest off the Paracas Peninsula. The evolution of the seismic moment release highlights two pulses, with the second larger and separated in time of ~60 s from the first one; without evidence of slow slip then this hiatus in the seismic radiation is likely due to a smaller sub-event (M_w 7.8) that dynamically triggered a second larger sub-event (M_w 8.0, Lay et al., 2010b). Such a kind of compound failure also occurred during the 2001 Peru M_w 8.4 earthquake.

The moderate size and depth (~20–40 km) of the slip patches contribute to generate a moderate tsunami generated striking only locally the Peruvian coast. Specifically, the coast of the southern side of the Paracas Peninsula, located in front of the main slip area and hence exposed to the tsunami leading wave, experienced the largest runups (5–7 m, maximum inundation distance of 2 km); conversely, the presence of small islands to the northwest of the peninsula attenuated the tsunami impact north of Paracas (average runups of 3 m).

Maule 2010

The subduction interface between the Nazca and South American Plates hosted on February 27, 2010 the M_w 8.8 Maule (central Chile) earthquake.

The source model of the Maule earthquake has been estimated by using joint inversions of different geophysical datasets, including geodetic data (GPS, InSAR, and land leveling), high-rate GPS, strong-motion, teleseismic waveforms, and tsunami data (e.g., Lay et al., 2010a; Lorito et al., 2011; Moreno et al., 2012). A common feature to all the models is the bilateral rupture propagation to the north and south of the epicenter (72.73°W, 35.91°S). The main slip patch (maximum slip of ~15–20 m) is located offshore north of the epicenter, whereas a second smaller (<10 m) patch is located to the south. Recent source models of the Maule earthquake estimated the presence of slip near the trench axis (e.g., Yue et al., 2014; Maksymowicz et al., 2017). The region interest by the 2010 Maule earthquake had previously been identified as a seismic gap (Madariaga et al., 2010) between the large events occurred in 1960 (M_w 9.5) to the south and in 1928 (M8.3) to the north of the epicenter. This portion of the plate boundary was shown by GPS observations to be characterized by strong plate coupling, commonly believed a proxy for the individuation of large coseismic slip occurrence. However, whereas the 2010 event nucleated within the gap, the large-slip were located outside.

The tsunami ensuing the 2010 Maule event hit ~600 km of the Chilean coast. The post-tsunami surveys measured runup with values in the rang ~3–30 m (Fritz et al., 2011), whose spatial distribution is well correlated the along-strike slip distribution. The steep morphology of the Chilean coast limited the tsunami inundation with a maximum penetration inland (~500 m) observed in Constitución. Very high runups were observed also in the Juán Fernández Archipelago (maximum runup of ~18 m measured on the coast of Robinson island), that is located in the perpendicular direction from the middle of the main patch of slip.

Tohoku 2011

The great Tohoku earthquake occurred on March 11, 2011, nucleating (142.37°E, 38.32°N) on the subduction interface between the Okhotsk and Pacific Plate. The earthquake magnitude of the event was M_w 9.1, making it is the largest Japanese seismic event ever recorded.

This earthquake, thanks to the huge amount of available seismic, geodetic, and tsunami data provided by the Japanese geophysical networks allowed to study the source process of a megathrust event from several points of view, enhancing the level of understanding about the subduction earthquakes. Indeed, more than 50 kinematic slip models (for a comprehensive review see Lay, 2017) were published, most of which share two main features: a spatially confined rupture area (<400 km) despite the earthquake magnitude (e.g., much less extended with respect to the 2004 Sumatra-Andaman or the 2010 Maule earthquakes that

have comparable magnitudes and rupture lengths of ~1300 km and ~650 km respectively), and very large amount of slip (>50 m) reaching the trench.

These features are at odds with classical empirical earthquake scaling laws (e.g., Strasser et al., 2010) and the common assumption that the shallow part of the megathrust shows an aseismic behavior due to the velocity-strengthening regime associate to the low rigidity materials characterizing the trench axis region. However, the outstanding results arising from the JFAST drilling project (Fulton et al., 2013 and references therein) suggested that the smectite-rich clays on the shallow part of megathrust, assuming high-slip rate (e.g., Faulkner et al., 2011), may have behaved as a slip velocity-weakening area thus allowing for a huge slip; the slip might be also have been amplified by dynamic effects due to the seismic waves reflection on the seafloor (Kozdon and Dunham, 2013).

The tsunami generated by the Tohoku earthquake was huge and exacerbated by the very large and shallow slip; consequently, the open ocean tsunami sensors recorded tsunami amplitudes >2 m (should be noticed that, generally, in the open ocean tsunami amplitude is a few tens of centimeters), whereas many Japanese tide gauges measured exceptional tsunami amplitudes >10 m (up to ~18 m at Onagawa). The tsunami struck mainly the coast of the Honshu island, where runups from ~10 to 40 m have been observed (Mori et al., 2011), and penetrating inland up to 5 km along the Sendai and Ishinomaki plains. The tsunami inundated also the Fukushima area, without possibility to retrieve measurements due to consequent nuclear accident.

Santa Cruz 2013

The plate boundary interface between the Australian and Pacific Plates hosted on February 6, 2013 an M_w 8.0 earthquake nearby Santa Cruz Islands whose hypocenter was located 76 km west of Lata (165.14°E, 10.64°S) at a depth of ~29 km.

The source process of this event has been studied by inverting teleseismic body waves optimized by forward modeling of DART tsunami signals (Lay et al., 2013a), teleseismic body and surface waves (Hayes et al., 2014), DART and tide-gauge tsunami signals (Romano et al., 2015). However, there are strong differences among these models due to using distinct datasets, fault geometries, and modeling assumptions. The model of Hayes et al. (2014) features less than 3.5 m on a single and quite deep slip patch, whereas the source model of Romano et al. (2015) places the main slip patch (~11 m) away from the hypocenter. The model of Lay et al. (2013a), featuring the rupture extending up to the seafloor, should, in principle, address and explain the differences between the other models being determined using both kinds of data.

The tsunami generated by this earthquake struck the coasts of Nendo Island with the maximum observed tsunami runup (>11 m, Fritz et al., 2014) located northeast of large coseismic slip regions and hence probably related to the direct arrival of the main tsunami waves. Lower runup observations (<3 m) were observed on the northwestern side of Nendo.

Iquique 2014

On April 1, 2014 a M_w 8.1 thrust earthquake occurred in Northern Chile with hypocenter located at 70.77°W, 19.61°S, depth 25 km rupturing the region of the Iquique seismic gap. This earthquake was preceded by an intense foreshock activity that lasted for several months and included a M_w 6.7 thrust event occurred 2 weeks before the mainshock. This earthquake was also followed by a large M_w 7.7 aftershock on April 3, with an epicenter located about 100 km southward (Schurr et al., 2014). The main shock generated a moderate tsunami that was recorded by Deep-ocean Assessment and Reporting of Tsunamis (DART) buoys in the Pacific Ocean (e.g., Heidarzadeh et al., 2014) and by several tide gauges along the chilean and peruvian coast (Gusman et al., 2015). No fatality was reported due to the tsunami although some damage to coastal areas was reported. Joint inversion of teleseismic waveforms, GPS offsets and strong motion data shows that the moment rate lasted for more than 130 s and was characterized by two main peaks, the first being larger than the second (Schurr et al., 2014). The major slip patch (up to 6.5 m) is located around the hypocenter, spanning 150 km along dip and 160 km along strike (Liu et al., 2015).

Illapel 2015

On 16 September 2015 at 22:54:32 (UTC), a large earthquake struck central Chile with a moment magnitude of M_w 8.4. The hypocenter (71.67°W, 31.57°S) was located at a depth of ~23 km along the subduction interface between the Nazca and South America plates. The area has been hit by a great earthquake in 1943, estimated to be slightly smaller at $M_w = 7.8–7.9$. The adjacent area to the north ruptured in 1922 in a much larger earthquake whereas to the south earthquakes in 1971 and 1985 broke the coupled interface and partially overlap with the 2010 Maule earthquake. This earthquake generated a tsunami that mainly struck the Chilean coasts from ~42°S to ~19°S with measured wave amplitudes up to some meters (4.7 m at the tide gauge in Coquimbo). The tsunami impact was significant (average observed runup >5 m (Contreras-López et al., 2016; Aránguiz et al., 2016) on a long stretch of the Chilean coast (>500 km), and in particular nearby Coquimbo (runup >10 m). However, the death toll has been very low, thanks to the evacuation of about one million people. Rapid analyses of the rupture process have been carried out soon after the earthquake by using short period teleseismic P wave back projection, indicating a northward rupture expansion from the hypocenter at a modest rupture velocity of 1.5–2.0 km/s (Ye et al., 2016). Further analysis, including joint inversion of InSAR and tsunami data, found that the coseismic slip was predominantly distributed to the NW of the hypocenter, with a maximum of ~9 m at ~15 km depth and significantly large slip (i.e., up to 5 m) in the shallow part of the megathrust (Romano et al., 2016).

Tsunamigenic Doublets

In seismology, doublet is a pair of (large) earthquakes of comparable size occurring over time close to each other (e.g., Lay and Kanamori, 1980). Two great doublets occurred in the period 2004–19, the first one involved an M_w 8.3 interplate earthquake on November 15, 2006 followed about 2 month later by an M_w 8.1 outer-rise earthquake (January 13, 2007) in the central Kuril Islands region; the second occurred on September 9, 2009 close to the Samoa islands and involved an M_w 8.1 outer-rise earthquake followed within a minute by an interplate M_w 8.0 event.

Understanding earthquake interactions causing these doublets is important for earthquake and tsunami hazard assessment. The doublets occurred in 2004–19 are particularly relevant because the Kuril doublet is the first documented case of a great ($M_w > 8$) and strongly tsunamigenic outer-rise event triggered by a thrust earthquake, whereas the Samoa doublet was the first documented case of a megathrust earthquake dynamically triggered by a great outer-rise event. However, some debate occurred regarding the earthquake temporal order of occurrence, and then on which event was triggered by the other.

Kurils 2006–07

The M_w 8.3 Kuril Islands earthquake occurred ~100 km southeast from the Simushir Island, with the hypocenter (153.32°E, 46.52°N) located on the shallow part of the subduction interface between the Pacific and Okhotsk Plates. The M_w 8.1 normal faulting earthquake (154.51°E, 46.08°N) occurred on January 13, 2007 in the outer-rise region of the 2006 event.

All source models for the 2006 earthquake (e.g., Lay et al., 2009; Fujii and Satake, 2008) estimate the rupture being propagated in the shallowest part the subduction interface with maximum slip from 8 to 13 m; the rupture zone estimated for the 2007 event is very narrow and features an average slip of ~7 m.

Both earthquakes generated tsunamis striking mostly uninhabited islands in the central area of the Kuril archipelago. The post-event survey was conducted after the 2007 earthquake, and therefore is difficult to distinguish to which of the two events the observations are associated. However, since there was an accumulation of snow in Kuril Islands during the 2007 event, this condition was not favorable for tsunami to erode the coast, and hence it is likely the runups observed (average value was ~10 m, maximum runup was 22 m) were related to the 2006 earthquake. The presence of cliffs along the coast limited the tsunami inundation distance (~20–500 m), whereas the islands in the area reduced the tsunami penetration into and propagation within the Sea of Okhotsk.

Samoa 2009

The Samoa doublet occurred on September 29, 2009 with an hypocenter (171.87°W, 15.53°S) located ~160 km southwest from the Samoa Islands at a depth of ~20 km.

While the analysis of GPS and tsunami data initially supported the hypothesis of an outer-rise earthquake triggered by an interplate rupture (similar to the 2006–07 Kuril double, Beavan et al., 2010), in-depth investigation of teleseismic data (Lay et al., 2010c) and back-projection analysis, demonstrated that this event was composed by an M_w 8.1 outer-rise earthquake followed by two thrust sub-events on the nearby plate boundary megathrust located ~50 km south of the normal faulting.

This earthquake generated a tsunami that struck the coasts of Samoa, American Samoa, and northern Tonga Islands with maximum runup in the range ~15–23 m and inundation distance of ~200–1000 m (Okal et al., 2010). In terms of source and propagation effects, the large inundation suffered by Pago Pago city (American Samoa) was due to the canyon-like bathymetric features offshore the city that have driven the tsunami toward the harbor where the wave was larger due to local amplification effects. Conversely, the presence of coral reefs extending ~2 km offshore reduced the tsunami impact on Niuatoputapu (Tonga), where the maximum runup reached ~10 m.

Tsunami Earthquakes

"Ordinary" interplate earthquakes are generally the largest seismic events, often generating devastating tsunamis. However, subduction zones also occasionally host another class of interplate seismic events called "tsunami earthquakes." These events generally nucleate along the megathrust at very shallow depths and generate tsunami larger than expected for their magnitude (commonly $M_w < 8$, Polet and Kanamori, 2016).

The seismic rupture of tsunami earthquakes is characterized by long duration, slow rupture velocity (~1.0–1.5 km/s), and large slip. The large slip featuring the tsunami earthquakes can be qualitatively explained by the presence of low rigidity materials (e.g., wet, low seismic velocity sediments) that allow for larger slip values for the same seismic moment than for high rigidity deeper rocks (i.e., at classical megathrust depth). Of course, this large shallow slip accounts for large seafloor displacement then resulting in a more efficient tsunami (Geist, 2009). Another feature related to the low rigidity is the weak ground motion that features these events; this does not favorite the self-evacuation of coastal population and along their frequency of occurrence represents a challenge for the tsunami warning systems and tsunami hazard assessment.

It should be stressed that the relatively weak ground shaking due to the depletion of source high frequency energy can exacerbate the tsunami impact because people are not prompted to self-evacuate; hence, tsunami preparedness campaigns should also point out that the duration of the shaking is very important and that has to be considered among the possible natural warnings of an imminent large tsunami.

The period 2004–19 was characterized by two tsunami earthquakes, the first occurred on 2006 in Java, the second on 2010 in Mentawai islands, both with M_w 7.8.

Java 2006

The shallow part of the subduction interface between the Australian and Sunda Plate hosted on July 17, 2006 an M_w 7.8 earthquake whose hypocenter was off the south coast of Java.

The source models of this event, studied using seismic (Ammon et al., 2006, Fig. 20) and tsunami (Fujii and Satake, 2006) data, share a slow rupture velocity (1–1.5 km/s) and the rupture extent (∼200–250 km) expanding unilaterally southeastward from the epicenter (107.32°E, 9.33°S) with most of the slip in the shallowest part of the megathrust. The 2006 earthquake generated a devastating tsunami that struck the coasts of Java.

The inundation along the coast is consistent with both the extent and the pattern of the seismic source featuring an average runup of 5–7 m with an inundation distance of ∼1 km (Fritz et al., 2008). A peak runup of 21 m was observed in Permisan city; this is probably due to the convex shape of the subduction nearby Java that may have led to a strong focusing effect of the tsunami toward Permisan.

Mentawai 2010

The M_w 7.8 Mentawai earthquake occurred on October 25, 2010 with the hypocenter (100.08°E, 3.46°S) located ∼40 km offshore southwest from the South Pagai Island.

The source models proposed for this earthquake share a pattern of slip mostly confined along the shallowest part of the megathrust (e.g., Yue et al., 2015 and references therein). The 2010 earthquake generated a large tsunami that struck the west coasts of the Mentawai Islands, with runup observations vary over a range of 2–17 m (Hill et al., 2012).

Whereas the largest runups (17 m) were observed on the Pagai Islands, that is in the near field of the seismic source, penetrating up to 600 m inland, on the other hand the same islands acted as a natural shield greatly mitigating the tsunami impact on cities like Padang on the Sumatran coast to the northeast.

Recent Special Cases

Sumatra 2012

Due to their mechanism, strike-slip earthquakes generally involve limited vertical seafloor displacement; hence, this kind of earthquakes are relatively low-tsunamigenic. This is the case for the April 11, 2012 M_w 8.7 Sumatra earthquake, that nucleated (92.82°E, 2.35°N) outside of the subduction zone some 100–200 km southwest of the Sunda Trench (∼300 km south from 2004 Sumatra earthquake epicenter). This seismic event, the largest intraplate earthquake ever recorded, was followed 2 h later by another strike-slip M_w 8.2 event, whose epicenter (92.31°E, 0.90°N) was ∼200 km south.

The source model of the M_w 8.72012 Sumatra earthquake has been estimated through teleseismic data inversion, highlighting peak slip of ∼37 m nearby the hypocenter, and a particularly high complexity of the seismic rupture; the rupture involved a system of orthogonal faults with both left- and right-lateral strike-slip mechanism (e.g., Yue et al., 2012; Hill et al., 2015).

As expected, even if the slip was very large, the tsunami generated was very modest due to the transcurrent faulting. It was recorded by several tide gauges in the Indian ocean with an average maximum wave amplitude smaller than 1 m. This kind of events are very challenging for tsunami warning systems because their high magnitude may lead to false alarms and they are generally events which were not considered in precomputed scenario databases, because they occur outside the subduction zone, in portions of oceanic crust characterized by low seismicity rates and possibly with unexpected faulting mechanisms.

Solomon 2007

The triple junction involving the Australian and Solomon Sea Plate underthrusting the Pacific Plate hosted on April 1, 2007 a M_w 8.1 interplate earthquake (156.58°E, 8.29°S) nearby the central Solomon Islands; this is the first well-documented case of a great event rupturing through a triple junction.

The source model of the 2007 Solomon earthquake has been investigated by inverting teleseismic (Furlong et al., 2009) or coral uplift and coastal subsidence data (Chen et al., 2009). These models share a similar pattern of slip characterized by two main shallow patches, one to the north of the triple junction with almost pure thrust mechanism (maximum slip is ∼7 m), the other one located to the south of the junction and featuring a slip direction with a strong oblique component (maximum slip is ∼4 m), consistently with the convergence direction of the Solomon Sea and Australia Plate, respectively.

The 2007 earthquake generated a tsunami that hit most of the islands in the Solomon archipelago with the maximum runup (~12 m) measured on the islands located within the vertical coseismic displacement field. The number of fatalities (60) was fortunately moderate thanks to the survivors of prior tsunamis that passed to the younger generations the message "run to high ground after an earthquake," thus significantly contributing to the self-evacuation (Fritz and Kalligeris, 2008).

Haida Gwaii 2012

On October 28, 2012, a M_w 7.8 shallow thrust earthquake occurred in the Haida Gwaii archipelago (Canada), whose hypocenter (131.93°W, 52.78°N) was located close to the Pacific coast beneath western Moresby Island; this is a transpressive boundary characterized by a predominantly right-lateral strike-slip motion between Pacific and North American Plate.

The source model of this event, inferred through teleseismic data inversion iteratively optimized by forward modeling of open ocean DART buoys tsunami waveforms (Lay et al., 2013b), indicates that most of the slip occurred offshore propagating up to the trench under the sedimentary wedge seaward of the Queen Charlotte Fault. Even though, apparently, this earthquake might be classified as a tsunami earthquake, despite the very shallow depth (i.e., low rigidity), its rupture velocity is not low (2.3 km/s), and the rupture does not feature significant low-frequency seismic radiation. Hence, the Haida Gwaii earthquake is not a tsunami earthquake.

This earthquake generated a tsunami that mainly struck the coast of Moresby Island. The observed runups are in the range of 3–13 m (Leonard and Bednarski, 2015) and are distributed coherently with the broadside of the tsunamigenic source, whereas the tsunami showed a limited inundation (up to ~60 m) due to steep coastal morphology.

Kaikoura 2016

On 13 November 2016, a M_w 7.8 earthquake struck the north-east coast of South Island New Zealand, in a zone characterized by oblique convergence between the Pacific and Australian plates. The hypocenter (173.05°E, 47.74°S, depth 15.1 km) was located about 60 km southwest of Kaikoura. Backprojection of high-frequency P waves shows unilateral rupture of at least two southwest-northeast striking faults with an average rupture speed of 1.4–1.6 km/s and total duration of ~100 s (Zhang et al., 2017): the rupture propagated northward for more than 170 m km along several faults before continuing offshore at its northeastern extent. Geodetic and field observations revealed an extremely complex rupture pattern, involving at least 12 major faults, including possible slip on the southern Hikurangi subduction interface, extensive uplift of the coastline and anelastic deformation of a rotated fault-bounded block (Hamling et al., 2017). Whether slip occurred on the subduction interface has been controversial, but seismic models (e.g., Bai et al., 2017; Duputel and Rivera, 2017; Wang et al., 2018) provide strong evidence that significant underthrusting below the crustal faulting did occur. This earthquake generated a tsunami well recorded at tide gauges along the eastern coasts and in Chatham Islands, including a ~4 m crest-to-trough signal at Kaikoura where coastal uplift was about 1 m, and at multiple gauges in Wellington Harbor (Bai et al., 2017). Though some of the existing fault models are able to reproduce the tsunami waveforms recorded by tide gauges, they tend to fail explaining runups up to 7 m at Kaikoura: for this reason, a submarine landslide has been suggested by some authors as an additional tsunami source to account for these observations (Heidarzadeh et al., 2019).

Mexico 2017

A great earthquake with M_w 8.2 (Global Centroid Moment Tensor solution) occurred offshore Chiapas and Oaxaca states, Mexico, on 8 September 2017 (15.022°N, 93.899°W, 47.4 km deep, 04:49:19.2 UTC, U.S. Geological Survey-National Earthquake Information Center). Rather than being a plate boundary thrust event in the regional Tehuantepec seismic gap, the faulting mechanism and depth indicate an intraslab normal fault rupture. Short-period back-projections indicate a largely unilateral rupture expansion toward the northwest, reaching to near the coastline (e.g., Meng et al., 2019). Inversion of teleseismic waveforms and iterative modeling of tsunami data indicate that the steeply dipping rupture extended ~180 km to the northwest along strike toward the Oaxaca coast and from ~30 to 70 km in depth, with peak slip of ~13 m (Ye et al., 2017). The rupture likely broke through the entire lithosphere in response to downdip slab pull and caused a local detachment of the young subducted slab (Ye et al., 2017; Melgar et al., 2018).The earthquake generated a tsunami with an amplitude of 1.8 m (height = 3.5 m) in Puerto Chiapas, Mexico. The tsunami was also observed at DART stations located in the deep ocean and at tide gauges located across the Pacific Ocean as far as 12,000 km from the epicenter (Gusman et al., 2018). Runup and inundation distances were measured along eight sites. The tsunami occurred at low tide and caused a maximum runup of about 3 m at Boca del Cielo and a maximum inundation distance of 190 m in Puerto Arista, corresponding to the coast in front of the epicenter and in the central sector of the Gulf of Tehuantepec (Ramirez-Herrera et al., 2017).

Palu 2018

On 28 September 2018 a M_w 7.5 earthquake occurred along the Palu-Koro fault system in the central area of Sulawesi, one of the four Greater Sunda islands (Indonesia), located at the triple junction between the Sunda, Australian, and Philippine Sea plates. The hypocenter of this earthquake was located ~70 km from the southern end of the Palu Bay (119.85°E, 0.18°S) at a depth of 20 km. Despite of the dominant strike-slip component of the faulting mechanism, as shown by the moment tensor solution, that in

principle should be not very effective in terms of tsunamigenesis, the earthquake was almost immediately followed by a significant tsunami that struck the coast of the entire Bay with devastating effects in terms of damages and fatalities (>2000). The earthquake rupture process has been investigated by inverting teleseismic body waves (Yolsal Çevikbilen and Taymaz, 2019), ground deformation from the Sentinel-2 satellite optical analysis (e.g., Socquet et al., 2019), and by a joint inversion of geodetic and the tsunami waveform recorded by the tide-gauge in Pantoloan within the Palu Bay (Gusman et al., 2019). Moreover, the results of back-projection of teleseismic waves highlighted a persistent supershear rupture propagating from the nucleation to the end of the rupture at a velocity greater than 4 km/s (Bao et al., 2019; Ulrich et al., 2019). Most of these seismic source models share a pattern of slip featuring the maximum coseismic dislocation in the middle of the Bay with values about 4–7 m. Interestingly, while preserving the dominant strike-slip character, some of these slip models find also a nonnegligible thrust component that produces seafloor uplift and thus in principle can be responsible for the tsunamigenesis. However, part of the runups observations collected during several post event surveys (e.g. Omira et al., 2019; Widiyanto et al., 2019) showing values in a range ~2–8 m, as well as the unusually short wave periods (<2 min) near the Palu city (reconstructed from video footages, Carvajal et al., 2019) are difficult to be reproduced with these rupture models; hence, the source of the tsunami following the 2018 Palu earthquake is still debated and some study does not rule out the contribution of a nonseismic source such as one or more submarine landslides to the causative source of this unexpected tsunami.

Conclusions

The last 15 years have witnessed a number of devastating tsunamigenic events. These events have demonstrated how the complexity of the source process, compound faulting, doublet events and "tsunami earthquakes" represent challenges for tsunami warning systems. However, these recent events have been recorded by vastly expanded seismic, geodetic, and tsunami networks whose data allow unprecedented analysis of these events and both enhancing understanding of the source processes and the tsunami excitation mechanisms. Of course, the worldwide instrumental coverage still has some limitations; not all events are observed with the same quality of recordings, but several collaborative initiatives are in progress to deploy additional instruments (such as ocean bottom pressure sensors and seafloor geodesy) and to increase the operational earthquake and tsunami warning capabilities in many regions. This will also allow rapid analysis of multiple datasets that have demonstrated to be effective when exploiting the complementary sensitivity to source processes provided by seismic, geodetic, and tsunami observation. Finally, the tsunamigenic earthquakes that occurred in the 2004–2019 period leave us with two important lessons: (i) tsunami hazard assessments need to consider not only "ordinary" interplate megathrust earthquakes but also "extreme" events such as those featuring very large shallow slip, "tsunami earthquakes" or intraplate ruptures in many regions; (ii) since the probabilities for these features/events are difficult to assess, great caution is needed concerning certain assumptions such as the earthquake segmentation or ruling out the possibility that an M9 earthquake may occur virtually on any subduction zone.

References

Ammon CJ, Kanamori H, Lay T, and Velasco AA (2006) The 17 July 2006 Java tsunami earthquake. *Geophysical Research Letters* 33: L24308. https://doi.org/10.1029/2006GL028005.

Aránguiz R, González G, González J, Catalán PA, Cienfuegos R, Yagi Y, Okuwaki R, Urra L, Contreras K, Del Rio I, and Rojas C (2016) The 16 September 2015 Chile tsunami from the post-tsunami survey and numerical modeling perspectives. *Pure and Applied Geophysics* 173: 333–348. https://doi.org/10.1007/s00024-015-1225-4.

Bai Y, Lay T, Cheung KF, and Ye L (2017) Two regions of seafloor deformation generated the tsunami for the 13 November 2016, Kaikoura, New Zealand earthquake. *Geophysical Research Letters* 44: 6597–6606. https://doi.org/10.1002/2017GL073717.

Bao H, Ampuero J-P, Meng L, Fielding EJ, Liang C, Milliner CWD, Feng T, and Huang H (2019) Early and persistent supershear rupture of the 2018 magnitude 7.5 Palu earthquake. *Nature Geoscience* 12: 200–205. https://doi.org/10.1038/s41561-018-0297-z.

Beavan J, Wang X, Holden C, Wilson K, Power W, Prasetya G, Bevis M, and Kautoke R (2010) Near-simultaneous great earthquakes at Tongan megathrust and outer rise in September 2009. *Nature* 466: 959–963. https://doi.org/10.1038/nature09292.

Borrero JC, Weiss R, Okal EA, Hidayat R, Arcas Suranto D, and Titov VV (2009) The tsunami of 2007 September 12, Bengkulu province, Sumatra, Indonesia: Post-tsunami field survey and numerical modelling. *Geophysical Journal International* 178: 180–194. https://doi.org/10.1111/j.1365-246X.2008.04058.x.

Briggs RW, Sieh K, Meltzner AJ, Natawidjaja D, Galetzka J, Suwargadi B, Hsu YJ, Simons M, Hananto N, Suprihanto I, Prayudi D, Avouac JP, Prawirodirdjo L, and Bock Y (2006) Deformation and slip along the Sunda megathrust in the great 2005 Nias-Simeulue earthquake. *Science* 311: 1897–1901. https://doi.org/10.1126/science.1122602.

Carvajal M, Araya-Cornejo C, Sepúlveda I, Melnick D, and Haase JS (2019) Nearly instantaneous tsunamis following the Mw 7.5 2018 Palu earthquake. *Geophysical Research Letters* 46: 5117–5126. https://doi.org/10.1029/2019GL082578.

Chen T, Newman AV, Feng L, and Fritz HM (2009) Slip distribution from the 1 April 2007 Solomon Islands earthquake: A unique image of the near-trench rupture. *Geophysical Research Letters* 36: L16307. https://doi.org/10.1029/2009GL039496.

Choi BH, Hong SJ, and Pelinovsky E (2006) Distribution of runup heights of the December 26, 2004 tsunami in the Indian Ocean. *Geophysical Research Letters* 33: L13601. https://doi.org/10.1029/2006GL025867.

Contreras-López M, Winckler P, Sepúlveda I, Andaur-Álvarez A, Córtes-Molina F, Guerrero CJ, Mizobe CE, Igualt F, Breuer W, Beyá JF, Vergara H, and Figueroa-Sterquel R (2016) Field survey of the 2015 Chile tsunami with emphasis on coastal wetland and conservation areas. *Pure and Applied Geophysics* 173: 349–367. https://doi.org/10.1007/s00024-015-1235-2.

Das S (2011) Earthquake rupture: Inverse problem. In: Gupta (ed.) *Encyclopedia of Solid Earth Geophysics*. Netherlands: Springer. https://doi.org/10.1007/978-90-481-8702-7.

Duputel Z and Rivera L (2017) Long-period analysis of the 2016 Kaikoura earthquake. *Physics of the Earth and Planetary Interiors* 265: 62–66. https://doi.org/10.1016/j.pepi.2017.02.004.

Faulkner DR, Mitchell TM, Behnsen J, Hirose T, and Shimamoto T (2011) Stuck in the mud? Earthquake nucleation and propagation through accretionary forearcs. *Geophysical Research Letters* 38: L18303. https://doi.org/10.1029/2011GL048552.

Fritz HM and Kalligeris N (2008) Ancestral heritage saves tribes during 1 April 2007 Solomon Islands tsunami. *Geophysical Research Letters* 35: L01607. https://doi.org/10.1029/2007GL031654.

Fritz HM, Kalligeris N, Borrero JC, Broncano P, and Ortega E (2008) The 15 August 2007 Peru tsunami runup observations and modeling. *Geophysical Research Letters* 35: L10604. https://doi.org/10.1029/2008GL033494.

Fritz HM, Petroff CM, Catalán CR, Winckler P, Kalligeris N, and Weiss R (2011) Field survey of the 27 February 2010 Chile tsunami. *Pure and Applied Geophysics* 168: 1989–2010. https://doi.org/10.1007/s00024-011-0283-5.

Fritz HM, Papantoniou A, Biukoto L, Gilly A, and Wei Y (2014) The Solomon Islands tsunami of 6 February 2013 in the Santa Cruz Islands: Field survey and modeling. In: *EGU General Assembly 2014, held 27 April - 2 May, in Vienna, Austria, id.15777.*

Fujii Y and Satake K (2006) Source of the July 2006 West Java tsunami estimated from tide gauge records. *Geophysical Research Letters* 33: L24317. https://doi.org/10.1029/2006GL028049.

Fujii Y and Satake K (2008) Tsunami sources of the November 2006 and January 2007 great Kuril earthquakes. *Bulletin of the Seismological Society of America* 98: 1559–1571. https://doi.org/10.1785/0120070221.

Fulton PM, Brodsky EE, Kano Y, Mori J, Chester F, Ishikawa T, Harris RN, Lin W, Eguchi N, Toczko S, and Expedition 343, 343T, and KR13-08 Scientists (2013) Low Coseismic friction on the Tohoku-Oki fault determined from temperature measurements. *Science* 342: 1214–1217. https://doi.org/10.1126/science.1243641.

Furlong KP, Lay T, and Ammon CJ (2009) A great earthquake rupture across a rapidly evolving three-plate boundary. *Science* 324: 226–229. https://doi.org/10.1126/science.1167476.

Geist EL (2009) Phenomenology of tsunamis: Statistical properties from generation to runup. *Advances in Geophysics* 51: 107–169. https://doi.org/10.1016/S0065-2687(09)05108-5.

Geist EL, Bilek SL, Arcas D, and Titov VV (2006) Differences in tsunami generation between the December 26, 2004 and March 28, 2005 Sumatra earthquakes. *Earth, Planets and Space* 58: 185–193. https://doi.org/10.1186/BF03353377.

Gusman AR, Murotani S, Satake K, Heidarzadeh M, Gunawan E, Watada S, and Schurr B (2015) Fault slip distribution of the 2014 Iquique, Chile, earthquake estimated from ocean-wide tsunami waveforms and GPS data. *Geophysical Research Letters* 42: 1053–1060. https://doi.org/10.1002/2014GL06260.

Gusman AR, Mulia IE, and Satake K (2018) Optimum sea surface displacement and fault slip distribution of the 2017 Tehuantepec earthquake (Mw 8.2) in Mexico estimated from tsunami waveforms. *Geophysical Research Letters* 45: 646–653. https://doi.org/10.1002/2017GL076070.

Gusman AR, Supendi P, Nugraha AD, Power W, Latief H, Sunendar H, et al. (2019) Source model for the tsunami inside Palu Bay following the 2018 Palu earthquake, Indonesia. *Geophysical Research Letters* 46: 8721–8730. https://doi.org/10.1029/2019GL082717.

Hamling IJ, et al. (2017) Complex multifault rupture during the 2016 Mw 7.8 Kaikoura earthquake, New Zealand. *Science* 356: 6334. https://doi.org/10.1126/science.aam7194.

Hayes GP, Furlong KP, Benz HM, and Herman HW (2014) Triggered aseismic slip adjacent to the 6 February 2013 M_w 8.0 Santa Cruz Islands megathrust earthquake. *Earth and Planetary Science Letters* 388: 265–272. https://doi.org/10.1016/j.epsl.2013.11.010.

Heidarzadeh M, Satake K, Murotani S, Gusman AR, and Watada S (2014) Deep-water characteristics of the trans-Pacific tsunami from the 1 April 2014 Mw 8.2 Iquique, Chile earthquake. *Pure and Applied Geophysics*. https://doi.org/10.1007/s00024-014-0983-8.

Heidarzadeh M, Tappin DR, and Ishibe T (2019) Modeling the large runup along a narrow segment of the Kaikoura coast, New Zealand following the November 2016 tsunami from a potential landslide. *Ocean Engineering* 175: 113–121. https://doi.org/10.1016/j.oceaneng.2019.02.024.

Hill EM, Borrero JC, Huang Z, Qiu Q, Banerjee P, Natawidjaja DH, Elosegui P, Fritz HM, Suwargadi BW, Pranantyo IR, Li LL, Macpherson KA, Skanavis V, Synolakis CE, and Sieh K (2012) The 2010 M_w 7.8 Mentawai earthquake: Very shallow source of a rare tsunami earthquake determined from tsunami field survey and near-field GPS data. *Journal of Geophysical Research* 117: B06402. https://doi.org/10.1029/2012JB009159.

Hill EM, Yue H, Barbot S, Lay T, Tapponnier P, Hermawan I, Hubbard J, Banerjee P, Feng L, Natawidjaja D, and Sieh K (2015) The 2012 M_w 8.6 Wharton Basin sequence: A cascade of great earthquakes generated by near-orthogonal, young, oceanic-mantle faults. *Journal of Geophysical Research* 120: 1–25. https://doi.org/10.1002/2014JB011703.

Hsu YJ, Simons M, Williams C, and Casarotti E (2011) Three-dimensional FEM derived elastic Green's functions for the coseismic deformation of the 2005 M_w 8.7 Nias-Simeulue, Sumatra earthquake. *Geochemistry, Geophysics, Geosystems* 12: 1–19. https://doi.org/10.1029/2011GC003553.

Kagan YY and Jackson DD (2013) Tohoku earthquake: A surprise? *Bulletin of the Seismological Society of America* 103: 1181–1194. https://doi.org/10.1785/0120120110.

Kanamori H (1977) The energy release of great earthquakes. *Journal of Geophysical Research* 82: 2981–2987.

Konca AO, Hjorleifsdottir V, Song TRA, Avouac JP, Helmberger DV, Ji C, Sieh K, Briggs R, and Meltzner A (2007) Rupture kinematics of the 2005 M_w 8.6 Nias-Simeulue earthquake from the joint inversion of seismic and geodetic data. *Bulletin of the Seismological Society of America* 97: S307–S322. https://doi.org/10.1785/0120050632.

Kozdon JE and Dunham EM (2013) Rupture to the trench: Dynamic rupture simulations of the 11 March 2011 Tohoku earthquake. *Bulletin of the Seismological Society of America* 103: 1275–1289. https://doi.org/10.1785/0120120136.

Lay T (2015) The surge of great earthquakes from 2004 to 2014. *Earth and Planetary Science Letters* 409: 133–146. https://doi.org/10.1016/j.epsl.2014.10.047 [Invited Frontiers Papers].

Lay T (2017) A review of the rupture characteristics of the 2011 Tohoku-oki M_W 9.1 earthquake. *Tectonophysics* 733: 4–36. https://doi.org/10.1016/j.tecto.2017.09.022.

Lay T and Kanamori H (1980) Earthquake doublets in the Solomon Islands. *Physics of the Earth and Planetary Interiors* 21: 283–304.

Lay T, Kanamori H, Ammon CJ, Hutko AR, Furlong K, and Rivera L (2009) The 2006–2007 Kuril Islands great earthquake sequence. *Journal of Geophysical Research* 114: B113208. https://doi.org/10.1029/2008JB006280.

Lay T, Ammon CJ, Kanamori H, Koper KD, Sufri O, and A R H (2010a) Teleseismic inversion for rupture process of the 27 February 2010 Chile (M_w 8.8) earthquake. *Geophysical Research Letters* 37: L13301. https://doi.org/10.1029/2010GL043379.

Lay T, Ammon CJ, Hutko AR, and Kanamori H (2010b) Effects of kinematic constraints on teleseismic finite-source rupture inversions: Great Peruvian earthquakes of 23 June 2001 and 15 august 2007. *Bulletin of the Seismological Society of America* 100: 969–994. https://doi.org/10.1785/0120090274.

Lay T, Ammon CJ, Kanamori H, Rivera L, Koper KD, and Hutko AR (2010c) The 2009 Samoa–Tonga great earthquake triggered doublet. *Nature* 466: 964–968. https://doi.org/10.1038/nature09214.

Lay T, Ye L, Kanamori H, Yamazaki Y, Cheung KF, and Ammon CJ (2013a) The February 6, 2013 M_w 8.0 Santa Cruz Islands earthquake and tsunami. *Tectonophysics* 608: 1109–1121. https://doi.org/10.1016/j.tecto.2013.07.001.

Lay T, Ye L, Kanamori H, Yamazaki Y, Cheung KF, Kwong K, and Koper KD (2013b) M_w 7.8 Haida Gwaii underthrusting earthquake and tsunami: Slip partitioning along the queen Charlotte fault transpressional plate boundary. *Earth and Planetary Science Letters* 375: 57–70. https://doi.org/10.1016/j.epsl.2013.05.005.

Leonard LJ and Bednarski JM (2015) The preservation potential of coastal coseismic and tsunami evidence observed following the 2012 M_w 7.8 Haida Gwaii thrust earthquake. *Bulletin of the Seismological Society of America* 105: 1280–1289. https://doi.org/10.1785/0120140193.

Liu C, Zheng Y, Wang R, and Xiong X (2015) Kinematic rupture process of the 2014 Chile Mw 8.1 earthquake constrained by strong-motion, GPS static offsets and teleseismic data. *Geophysical Journal International* 202: 1137–1145. https://doi.org/10.1093/gji/ggv214.

Lorito S, Romano F, Piatanesi A, and Boschi E (2008) Source process of the September 12, 2007, M_w 8.4 southern Sumatra earthquake from tsunami tide gauge record inversion. *Geophysical Research Letters* 35: L02310. https://doi.org/10.1029/2007GL032661.

Lorito S, Romano F, Atzori S, Tong X, Avallone A, McCloskey J, Cocco M, Boschi E, and Piatanesi A (2011) Limited overlap between the seismic gap and coseismic slip of the great 2010 Chile earthquake. *Nature Geoscience* 4: 173–177. https://doi.org/10.1038/ngeo1073.

Lorito S, Romano F, and Lay T (2016) Tsunamigenic earthquakes (2004–2013): Source processes from data inversion. Solicited paper. In: Meyers RA (ed.) *Encyclopedia of Complexity and Systems Science*. New York: Springer Science + Business Media. https://doi.org/10.1007/978-3-642-27737-5_641-1.

Madariaga R, Métois M, Vigny C, and Campos J (2010) Central Chile finally breaks. *Science* 328: 181–182. https://doi.org/10.1126/science.1189197.

Maksymowicz A, Chadwell CD, Ruiz J, Tréhu AM, Contreras-Reyes E, Weinrebe W, et al. (2017) Coseismic seafloor deformation in the trench region during the M_w 8.8 Maule megathrust earthquake. *Scientific Reports* 7: 45918. https://doi.org/10.1038/srep45918.

Melgar D, Ruiz-Angulo A, Garcia ES, Manea M, Manea VC, Xu X, Ramirez-Herrera MT, Zavala-Hidalgo J, Geng J, Corona N, Pérez-Campos X, Cabral-Cano E, and Ramirez-Guzmán L (2018) Deep embrittlement and complete rupture of the lithosphere during the Mw 8.2 Tehuantepec earthquake. *Nature Geoscience* 11: 955–960. https://doi.org/10.1038/s41561-018-0229-y.

Meng L, Huang H, Xie Y, Bao H, and Dominguez LA (2019) Nucleation and kinematic rupture of the 2017 Mw 8.2 Tehuantepec earthquake. *Geophysical Research Letters* 46(7): 3745–3754. https://doi.org/10.1029/2018GL081074.

Moreno M, Melnick D, Rosenau M, Baez J, Klotz J, Oncken O, Tassara A, Chen J, Bataille K, Bevis M, Socquet A, Bolte J, Vigny C, Brooks B, Ryder I, Grund V, Smalley B, Carrizo D, Bartsch M, and Hase H (2012) Toward understanding tectonic control on the M_w 8.8 2010 Maule Chile earthquake. *Earth and Planetary Science Letters* 321-322: 152–165. https://doi.org/10.1016/j.epsl.2012.01.006.

Mori N, Takahashi T, Yasuda T, and Yanagisawa H (2011) Survey of the 2011 Tohoku earthquake tsunami inundation and runup. *Geophysical Research Letters* 38: L00G14. https://doi.org/10.1029/2011GL049210.

Okal EA, Fritz HM, Synolakis CE, Borrero JC, Weiss R, Lynett PJ, Titov VV, Foteinis S, Jaffe BE, Liu PLF, and Chan I (2010) Field survey of the Samoa tsunami of 29 September 2009. *Seismological Research Letters* 81: 577–591. https://doi.org/10.1785/gssrl.81.4.577.

Omira R, et al. (2019) The September 28th, 2018, tsunami in Palu-Sulawesi, Indonesia: A post-event field survey. *Pure and Applied Geophysics* 176: 1379–1395. https://doi.org/10.1007/s00024-019-02145-z.

Piatanesi A and Lorito S (2007) Rupture process of the 2004 Sumatra-Andaman earthquake from tsunami waveform inversion. *Bulletin of the Seismological Society of America* 97: S223–S231. https://doi.org/10.1785/0120050627.

Plafker G, Nishenko S, Cluff L, and Syahrial M (2006) The cataclysmic 2004 tsunami on NW Sumatra—Preliminary evidence for a near-field secondary source along the western Aceh basin. *Seismological Research Letters* 77: 231.

Polet J and Kanamori H (2016) Tsunami earthquakes. In: Meyers RA (ed.) *Encyclopedia of Complexity and Systems Science*, pp. 9577–9592. Berlin Heidelberg: Springer Publishing. https://doi.org/10.1007/978-3-642-27737-5_567-2.

Ramirez-Herrera MT, Corona N, Ruiz-Angulo A, Melgar D, and Zavala-Hidalgo J (2017) The 8 September 2017 tsunami triggered by the Mw 8.2 intraplate earthquake, Chiapas, Mexico. *Pure and Applied Geophysics* 175: 25–34. https://doi.org/10.1007/s00024-017-1765-x.

Romano F, Piatanesi A, Lorito S, D'Agostino N, Hirata K, Atzori S, Yamazaki Y, and Cocco M (2012) Clues from joint inversion of tsunami and geodetic data of the 2011 Tohoku-Oki earthquake. *Scientific Reports* 2: 385. https://doi.org/10.1038/srep00385.

Romano F, Molinari I, Lorito S, and Piatanesi A (2015) Source of the 6 February 2013 M_w 8.0 Santa Cruz Islands tsunami. *Natural Hazards and Earth System Sciences* 15: 1371–1379. https://doi.org/10.5194/nhess-15-1371-2015.

Romano F, Piatanesi A, Lorito S, Tolomei C, Atzori S, and Murphy S (2016) Optimal time alignment of tide-gauge tsunami waveforms in nonlinear inversions: Application to the 2015 Illapel (Chile) earthquake. *Geophysical Research Letters* 43. https://doi.org/10.1002/2016GL071310.

Satake K (2009) Tsunamis, inverse problem of. In: Meyers A (ed.) *Encyclopedia of Complexity and Systems Science*. New York: Springer.

Schurr B, et al. (2014) Gradual unlocking of plate boundary controlled initiation of the 2014 Iquique earthquake. *Nature* 512: 299–302. https://doi.org/10.1038/nature13681.

Shearer P and Bürgmann R (2010) Lessons learned from the 2004 Sumatra-Andaman megathrust rupture. *Annual Review of Earth and Planetary Sciences* 38: 103–131. https://doi.org/10.1146/annurev-earth-040809-152537.

Sieh K, McKinnon EE, Pilarczyk JE, Chiang HW, Horton B, Rubin CM, Shen CC, Ismail N, Vane CH, and Feener RM (2015) Penultimate predecessors of the 2004 Indian Ocean tsunami in Aceh, Sumatra: Stratigraphic, archeological, and historical evidence. *Journal of Geophysical Research* 120: 308–325. https://doi.org/10.1002/2014JB011538.

Sladen A, Tavera H, Simons M, Avouac JP, Konca AO, Perfettini H, Audin L, Fielding EJ, Ortega F, and Cavagnoud R (2010) Source model of the 2007 M_w 8.0 Pisco, Peru earthquake—Implications for seismogenic behavior of subduction megathrusts. *Journal of Geophysical Research* 115: B02405. https://doi.org/10.1029/2009JB006429.

Socquet A, Hollingsworth J, Pathier E, and Bouchon M (2019) Evidence of supershear during the 2018 magnitude 7.5 Palu earthquake from space geodesy. *Nature Geoscience* 12: 192–199. https://doi.org/10.1038/s41561-018-0296-0.

Stein S and Okal EA (2011) The size of the 2011 Tohoku earthquake need not have been a surprise. *Eos* 92: 227–228.

Strasser FO, Arango MC, and Bommer JJ (2010) Scaling of the source dimensions of interface and intraslab subduction-zone earthquakes with moment magnitude. *Seismological Research Letters* 81: 941–950.

Titov V, Rabinovich AB, Mofjeld HO, Thomson RE, and González FI (2005) The global reach of the 26 December 2004 Sumatra tsunami. *Science* 309: 2045–2048. https://doi.org/10.1126/science/1114576.

Ulrich T, Vater S, Madden EH, Behrens J, Van Dinther Y, Van Zelst I, Fielding EJ, Liang C, and Gabriel A-A (2019) Coupled, physics-based modeling reveals earthquake displacements are critical to the 2018 Palu, Sulawesi tsunami. *Pure and Applied Geophysics* 176: 4069–4109. https://doi.org/10.1007/s00024-019-02290-5.

Wang K and Kinoshita M (2013) Dangers of being thin and weak. *Science* 342. https://doi.org/10.1126/science.1246518.

Wang T, Wei S, Shi X, Qiu Q, Li L, Peng D, Weldon RJ, and Barbot S (2018) The 2016 Kaikōura earthquake: Simultaneous rupture of the subduction interface and overlying faults. *Earth and Planetary Science Letters* 482: 44–51. https://doi.org/10.1016/j.epsl.2017.10.056.

Widiyanto W, Santoso PB, Hsiao S-C, and Imananta RT (2019) Post-event field survey of 28 September 2018 Sulawesi earthquake and tsunami. *Natural Hazards and Earth System Sciences* 19: 2781–2794. https://doi.org/10.5194/nhess-2019-91.

Ye L, Lay T, Kanamori H, and Koper KD (2016) Rapidly estimated seismic source parameters for the 16 September 2015 Illapel, Chile Mw 8.3 earthquake. *Pure and Applied Geophysics* 173: 321–332. https://doi.org/10.1007/s00024-015-1202-y.

Ye L, Lay T, Bai Y, Cheung KF, and Kanamori H (2017) The 2017 Mw 8.2 Chiapas, Mexico, earthquake: Energetic slab detachment. *Geophysical Research Letters* 44: 11824–11832. https://doi.org/10.1002/2017GL076085.

Yolsal-Çevikbilen S and Taymaz T (2019) Source characteristics of the 28 September 2018 Mw 7.5 Palu-Sulawesi, Indonesia (SE Asia) earthquake based on inversion of teleseismic bodywaves. *Pure and Applied Geophysics* 176: 4111–4126. https://doi.org/10.1007/s00024-019-02294-1.

Yue H, Lay T, and Koper KD (2012) En échelon and orthogonal fault ruptures of the 11 April 2012 great intraplate earthquakes. *Nature* 490: 245–249. https://doi.org/10.1038/nature11492.

Yue H, Lay T, Rivera L, An C, Vigny C, Tong X, and Báez Soto JC (2014) Localized fault slip to the trench in the 2010 Maule, Chile $M_w = 8.8$ earthquake from joint inversion of high-rate GPS, teleseismic body waves, InSAR, campaign GPS, and tsunami observations. *Journal of Geophysical Research* 119: 1–19. https://doi.org/10.1002/2014JB011340.

Yue H, Lay T, Li L, Yamazaki Y, Cheung KF, Rivera L, Hill EM, Sieh K, Kongko W, and Muhari A (2015) Validation of linearity assumptions for using tsunami waveforms in joint inversion of kinematic rupture models: Application to the 2010 Mentawai M_w 7.8 tsunami earthquake. *Journal of Geophysical Research* 120: 1728–1747. https://doi.org/10.1002/2014JB011721.

Zhang H, Koper KD, Pankow K, and Ge Z (2017) Imaging the 2016 Mw 7.8 Kaikoura, New Zealand, earthquake with teleseismic P waves: A cascading rupture across multiple faults. *Geophysical Research Letters* 44: 4790–4798. https://doi.org/10.1002/2017GL073461.

Further Reading

Grezio A, Babeyko A, Baptista MA, Behrens J, Costa A, Davies G, et al. (2017) Probabilistic tsunami Hazard analysis: Multiple sources and global applications. *Reviews of Geophysics* 55: 1158–1198. https://doi.org/10.1002/2017RG000579.

Løvholt F, et al. (2019) Global trends in advancing tsunami science for improved hazard and risk understanding. In: *Contributing Paper to GAR 2019* .

UNDRR (2019) *Global Assessment Report on Disaster Risk Reduction*. Geneva, Switzerland: United Nations Office for Disaster Risk Reduction (UNDRR).

Beroza GC and Kanamori H (2015) Treatise on Geophysics, Reference Work. *Earthquake Seismology*, 2nd edn., vol. 4. Amsterdam: Elsevier.

Relevant Websites

https://earthquake.usgs.gov/earthquakes/—USGS earthquake catalogue.
https://www.ngdc.noaa.gov/hazard/tsu_db.shtml—NGDC/WDS Global Historical Tsunami Database.
https://www.jamstec.go.jp/chikyu/e/exp343/science.html—JFAST drilling project.